Journal of the Indian Institute of Science
A Multidisciplinary Reviews Journal
ISSN: 0970-4140 Coden-JIISAD

REVIEWS

Spectrally Encoded Confocal Microscopy: A New Paradigm for Diagnosis

Parama Pal

Abstract | Since its invention in 1955 by Marvin Minsky, confocal microscopy has become an indispensable tool for biomedical imaging at high resolutions. Dramatic progress in optical fiber technology has propelled its translation from the benchtop to the bedside in the form of clinical confocal endomicroscopy. The optical sectioning capability, which is central to confocal microscopy, renders this technique as a versatile diagnostic tool that provides images similar to histology and is thus uniquely well-suited for non invasive microscopy in *vivo*. Reflectance confocal microscopy (RCM) is a special case of confocal microscopy, which derives structural information of the sample from backscattered light and does not use any external contrast agents. A variant of RCM, known as spectrally encoded confocal microscopy (SECM), obtains images at speeds that are nearly ten times faster than video rate. This technique, described in this review paper, can be used to guide biopsies efficiently and vastly improve diagnostic yields in clinical scenarios.

1 Introduction

The gold standard for the diagnosis of many disease conditions such as malignant or premalignant lesions is the microscopic examination of excised tissue obtained through biopsies from the region at risk. Excisional biopsies, i.e., when tissue from a suspected disease site is excised or removed for further pathological inspection under an optical microscope, are typically performed when conventional visual inspection, standard white light endoscopy, or radiologic techniques are unable to verify the presence of disease. For several clinical scenarios, such as the screening and surveillance of large tissue areas, excisional biopsy is not a practice free from flaws.[1] The procedure involves random sampling of the suspect site and is thus, inherently fraught with sampling errors. Additionally, traditional biopsy methods for diagnosis of disease are surgically invasive, may cause bleeding, perforation or infection, and are often difficult for the patient to tolerate. Also, a significant turnaround time for results is involved due to the steps involved in the tissue preparation process prior to microscopic examination such as formalin fixation, paraffin embedding followed by preparation of thin slices of the specimen with a microtome, dye staining after the paraffin is removed, and finally mounting on a glass slide.[2] Several well-established noninvasive imaging modalities such as magnetic resonance imaging (MRI) and computed tomography (CT) have the ability to image the entire body but do not have the resolution required for visualizing the morphological and cellular changes of early cancerous and precancerous conditions. There is a need to develop a technique that can effectively 'guide' traditional biopsy procedures to reduce the errors associated with them and provide diagnoses that are more representative of the true disease state. An optical biopsy entails comprehensively imaging large tissue areas using optical methods, and is a relatively new technique that strives to provide the physician with real-time cellular images from a minimally invasive endoscopic procedure.

Confocal laser endomicroscopy (CLE) is an adaptation of confocal microscopy, which is implemented via an endoscope. The confocal imaging microscope was first conceptualized and patented

Magnetic resonance imaging (MRI): An imaging technique that uses the property of nuclear magnetic resonance (NMR) to image nuclei of atoms inside the body.

Computed tomography (CT): A medical imaging procedure that uses X-rays to produce tomographic images or 'slices' of specific areas of the body.

The Robert Bosch Centre for Cyber Physical Systems, Indian Institute of Science, Bangalore 560012, India.
**ppal@cps.iisc.ernet.in*

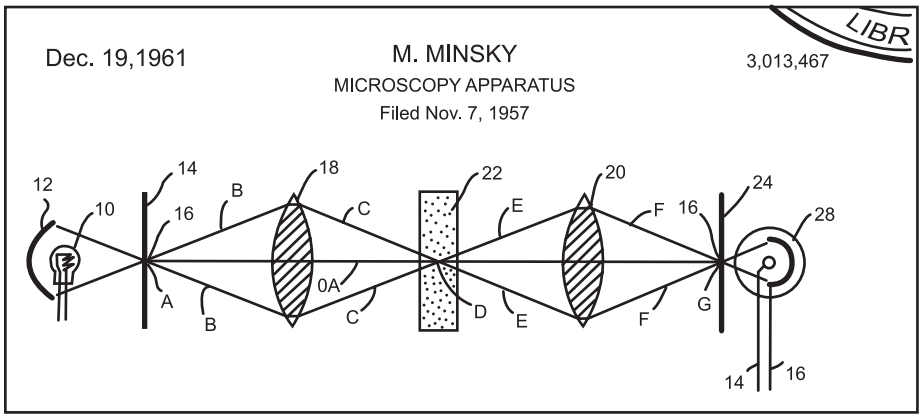

Figure 1: First page of patent/schematic of confocal principle.[3]

by Marvin Minsky at Harvard University in 1955 (Figure 1).[3,4] For many years, confocal microscopy has been an indispensable research tool for the identification and characterization of subcellular microstructures of excised specimens. Typical configurations involve a low-power laser, which is focused onto a single point in a defined microscopic field of view by an objective lens, and the same lens is used as both the condenser and objective folding optical path. The point of illumination thus coincides with the point of detection within the specimen. The use of a small, limiting aperture (pinhole) positioned at the image plane of the objective ensures that only the light originating from the focal spot passes to the detector to provide the signal for one pixel and light from outside the illuminated spot is rejected; this enhances lateral resolution and reduces depth of field as compared to conventional white light microscopy.[5,6] Since the illumination and detection apertures are in optically conjugate focal planes, i.e., they are positioned at optically conjugated points of the ray path, they are termed 'confocal'. The image of a scanned region is constructed and digitized by measuring the light returning to the detector from successive points. Single points are typically scanned in a raster pattern. Optical 'slices' of the sample (consisting of reflected light) are collected and thus, a stack of depth-resolved optical images are obtained without any physical sectioning.

Most forms of CLE in the past have relied on fluorescence and have involved the administration of fluorescence contrast agents, such as fluorescein and acriflavine, applied either intravenously or topically.[7-10] However, if exogenous contrast agents are to be avoided, an ideal candidate for 'smart' optical biopsies is reflectance confocal microscopy (RCM), which is based on the confocal selection of singly backscattered photons from the sample of interest (biological tissue in this case). The source of contrast for RCM is provided by the refractive index variations between the cell nucleus and cytoplasm.[11,12] By virtue of the optical sectioning capability, 'virtual' histology slides can be obtained rapidly. Confocal microscopes typically, can capture high-resolution images from a specific plane in the tissue up to a few hundred micrometers below the surface. Since many cancers, especially in regions such as the esophagus, are epithelial,[8,13–15] the confocal technique is an excellent choice for optical biopsy. For adapting RCM in a clinical setting, a few important requirements must be satisfied: first, a focused beam must be scanned across the specimen. Second, the image acquisition time has to be sufficiently short to prevent motion artifacts. Finally, the imaging device must be small enough to be incorporated into an endoscope or catheter.[16,17] Early embodiments of confocal scanning reflectance microscopy involved mechanisms for enabling scanning in two orthogonal directions, such as fast rotating polygonal mirrors[18] and oscillating galvanometric mirrors.[19] Sufficiently fast scanners such as spinning polygons are difficult to miniaturize, however, and the substantial technical challenges involved in developing a scanning mechanism appropriate for *in vivo* probes, for a while, limited the utility of confocal microscopy to the fields of dermatology and ophthalmology.

2 SECM—The Basic Principles

Spectrally encoded confocal microscopy (SECM), is a fiber-based, confocal imaging method that uses multiple wavelengths to encode spatial information.[20] It is a technique that uses the aperture of a single optical fiber as a spatial filter for the confocal selection of light. Since multiple wavelengths are required, the source can either be a broadband source or a wavelength-swept source. The spectral encoding is analogous to the principle

of wavelength division multiplexing wherein the illumination from a multi-wavelength source is dispersed into its constituents by an appropriate dispersive optical element (typically a transmission diffraction grating), which is subsequently focused using an objective lens to a line (Figure 2). This transverse line focus is essentially the locus of focal points corresponding to each wavelength in the illuminating spectrum. The objective lens is placed distal to the optical fiber and the spectrally encoded line is scanned in the orthogonal dimension on the sample.

The optical fiber has two purposes: as a conduit for the illumination (both incident as well as back-scattered) and as a spatial filter for rejecting out-of-focus light through its aperture/end facet. The spectrum of the light remitted from the sample is decoded/de-scanned to yield the reflectance as a function of transverse displacement within the sample. The spectral encoding provides a means to reduce the number of physical scanners by replacing/obviating one dimension of scanning whereas the orthogonal scan dimension is obtained via mechanical actuation. This scheme yields two major advantages: it significantly simplifies the construction of SECM probe designs and effectively increases the scan speed by nearly an order of magnitude owing to the elimination of the need to scan both directions to image the sample.

2.1 *Optical performance*

For a typical SECM system, light from the source is guided through an optical fiber. The output from the fiber, after collimation, is made incident on a high-groove density diffraction grating at Littrow's angle, i.e., an angle at which the light is diffracted back along the incident beam. In a Littrow configuration, the grating equation, namely,

$$gm\lambda = (\sin\alpha + \sin\beta_m) \quad (1)$$

Diffraction grating: A collection of reflecting (or transmitting) elements spaced by distances of the order of the wavelength of interest.

where, g is the groove density or groove frequency and is the reciprocal of the line spacing/pitch, m is the diffraction or spectral order (integer), α is the angle of incidence and β_m is the diffraction angles(s) (all angles measured relative to the grating normal), reduces to,

$$gm\lambda = 2\sin\alpha \quad (2)$$

since α equals β. For a source with a finite bandwidth given by $\Delta\lambda$, the total number of resolvable points, 'N', for the first diffraction order ($m = 1$) is defined by,

$$N = \Delta\lambda(d)(g)/\lambda_0 \quad (3)$$

where, $\Delta\lambda$ is the source bandwidth, λ_0 is the center wavelength, and d is the input beam diameter.

The lateral resolution is then given by the ratio of the field of view to the total number of resolvable spots, i.e.,

$$\Delta x = \mathrm{FOV}/N \quad (4)$$

The resolving power R of a grating is a measure of its ability to separate the adjacent spectral lines of average wavelength λ. It is usually expressed as the dimensionless quantity $(\lambda/\Delta\lambda)$. Here $\Delta\lambda$ is the limit of resolution, the difference in wavelength between two lines of equal intensity that can be distinguished, and is often described by the

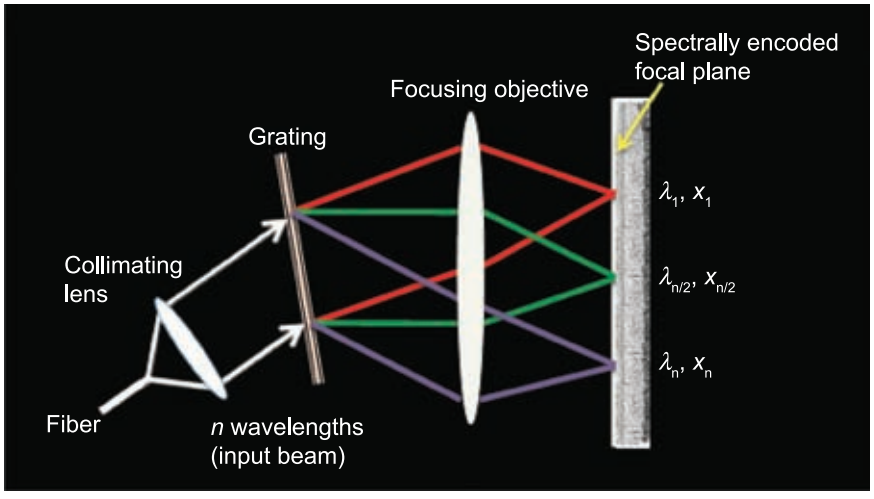

Figure 2: Schematic of the SECM concept.

Rayleigh's criterion, which states that the intensity of maxima of two neighboring wavelengths are resolvable if the intensity maximum of one wavelength coincides with the intensity minimum of the other. It is also expressed theoretically by $R = mN$, where, N is the number of grooves illuminated on the grating surface. In a Littrow configuration, the maximum attainable resolving power of the grating is achieved.

From the Rayleigh's criterion, the lateral resolution of a conventional confocal microscope is deduced as,[5]

$$\Delta x_{conf} = 0.41\ \lambda/\mathrm{NA} \quad (5)$$

Numerical aperture: The numerical aperture of a microscope objective is a measure of its ability to gather light. Mathematically, it is the sine of the acceptance angle of a waveguide or fiber.

where, NA is the numerical aperture of the objective. For an SECM system, several factors contribute to the overall lateral resolution, namely, the resolving power of the grating in the imaging arm, the size of the focal spot produced by the objective, and, for a system based on a wavelength-swept source, the instantaneous line-width of the source.[21] The resultant resolution, however, is governed by the element with the poorest resolution. The spectral resolution of an SECM system may be given in terms of resolvable points (bandwidth/linewidth). Finally, as the resolving power of the grating in the imaging arm is given by $R = \lambda/\Delta\lambda$, and it can be shown that,

$$R = \lambda/\Delta\lambda = mD/L \quad (6)$$

1951 USAF resolution target: A resolution test pattern conforming to the MIL-STD-150A standard set by US Air Force in 1951 consisting of groups of three bars with varying dimensions.

Ronchi ruler: A constant-interval bar and space square wave optical target used widely for optical testing purposes that has a high edge definition and contrast ratio.

where, L is the grating period.

Along the wavelength axis, the field of view (FOV) is given by:

$$\mathrm{FOV} = 2f \tan(\Delta\theta/2) \quad (7)$$

where, f is the effective focal length of the objective lens and $\Delta\theta$ is the deviation from Littrow's angle due to bandwidth of the source and obtained after taking the derivative of the grating equation,

$$\Delta\theta = m\Delta\lambda/\cos\theta.\ \Lambda \quad (8)$$

Experimentally, the lateral/transverse resolution is often measured in terms of an 'edge-response' function. In this technique, the source is presented with an object that transmits radiation on one side of an edge but is perfectly attenuating on the other, i.e., an object whose transmission is described by a step function. The edge-spread function is the image of the step object. The line spread function can be derived as the spatial derivative of the edge spread function and the lateral resolution is inferred from it.[22] It can also be estimated by observing the smallest bars on a 1951 USAF resolution target that can be resolved (Figure 3a).

The axial resolution, rather, the optical sectioning, is measured by translating a surface, such as a high-reflectivity mirror through the focal plane of the objective lens and then plotting the remitted signal intensity as a function of the axial displacement. The full width at half maximum of the plotted function gives the axial resolution of the confocal system. The field width is estimated by counting the number of lines observed when a diffraction grating or Ronchi ruling is imaged (Figure 3b).

The choice of light source determines the detection scheme required for SECM. For a broadband light source, a spectrometer is used which is typically assembled with a diffraction grating followed by a lens to focus the light onto a high-speed line scan camera. When a wavelength-swept light source is used, a fast InGaAs (indium gallium arsenide) photodiode measures the captured light intensity.

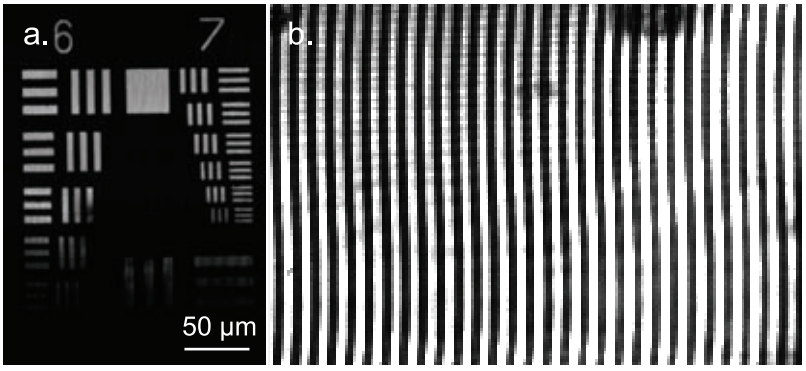

Figure 3: a. SECM image of a 1951 Air Force resolution target for determination of lateral resolution. b. SECM image of a Ronchi ruler to measure field of view.

3 System Components

In 1998, Tearney et al. were the first to demonstrate the concept of spectral encoding for fiber-optic confocal imaging.[20] Their setup was based on a 75 nm-wide quasi-monochromatic superluminescent diode (SLED) centered at 904 nm as the illumination source for the system. A total output power of 460 μwatt was guided through a fiber-optic 3-dB coupler to the sample stage where it was collimated to a beam with a diameter of 12 mm. The probe prototype, which consisted of a blazed grating in conjunction with a water immersion microscope objective (30X, 0.9-NA), had an overall working distance of 1.5 mm. Approximately 300 points were resolved by the grating (as determined by equation 3). The image was reconstructed by decoding the confocal remittance via heterodyne Fourier-transform spectroscopy (FTS) by inserting a linearly translating mirror into the reference arm and measuring the cross-correlation output from the interferometer. One full spectrum, i.e., for the acquisition of one complete line of the image, the scan rate was 2.72 Hz. The signal acquired was digitized and subsequently Fourier transformed to generate the confocal reflectivity information. The orthogonal dimension was scanned by a computer controlled stepper motor stage. The measured value of the approximate minimal lateral resolvable distance for the wavelength-encoded axis was 0.78 ± 0.04 μm. This first demonstration paved the way for later adaptations of SECM with enhanced imaging capabilities that yielded sufficient cellular details for diagnostic interpretation.

A general SECM imaging system (depicted in Figure 4) can be broken down into two major components, namely, the console and the probe. The console houses the light source, detectors (spectrometer or photodetector), additional electronics, as well as the data recording system and is typically stored within a portable cart that can be conveniently moved to any location especially within a clinical setting. A third component may be introduced in the form of scanning mechanisms such as a MEMS (microelectromechanical) scanner or an appropriate interface between the probe and the console. Numerous optical imaging studies, such as OFDI (described later), for instance, have involved the use of custom rotary junctions, which essentially couples a static fiber apparatus to a rotating one that resides within the imaging head and enables it to scan rapidly in a circular motion.

3.1 *Imaging probes*

Clinical settings have benefitted tremendously from progress in the fields of miniaturized optics and fiber-optics, advances which contribute greatly towards reducing the size of the device and increasing its functionality.[14,23] Fiber-optic devices, owing to their compact form factor and robustness, can access regions such as hollow tissue cavities (such as the GI tract) and hence enable imaging where conventional light microscopy cannot be used.[15,18,24–29] The aperture of a single-mode fiber in effect, replaces the pinhole, which provides optical sectioning in a conventional tabletop confocal microscope. It also decouples the imaging arm from the light source and detector since it acts as both the illumination and detection pinholes. The basic utility of an optical fiber is mainly that of a conduit; optical fibers deliver, and in the case of imaging probes, collect remittance from the sample. Optical fibers are also lightweight and inexpensive. The development of a probe is central to imaging modalities such as RCM for

Superluminescent light emitting diode (SLED): An optoelectronic semiconductor light source based on amplified spontaneous emission, which combines the high power and brightness of laser diodes with the low coherence of conventional LEDs.

Microelectromechanical (MEMS): A technology defined by miniaturized (<1 μm to a few millimeters) mechanical and electromechanical devices and structures (microsensors, microactuators, microelectronics) that are made using specialized microfabrication techniques.

Blazed grating: Gratings that are optimized to achieve maximum efficiency in a given diffraction order. The direction in which maximum efficiency is achieved is called the *blaze angle*.

Fourier-transform spectroscopy (FTS): A measurement technique whereby spectra are collected based on measurements of the coherence of a radiative source via interferometry.

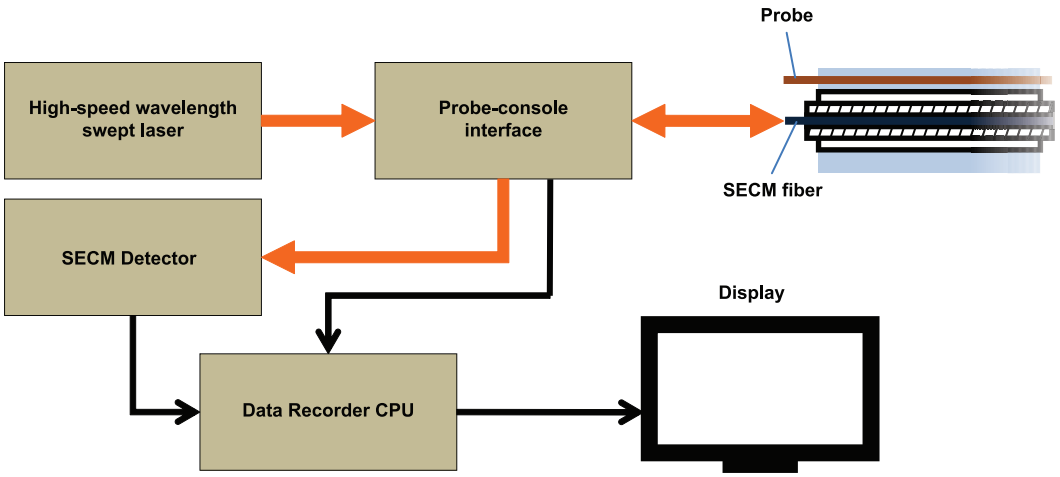

Figure 4: Schematic of an SECM imaging system.

in vivo use. Considerable efforts have been channeled into designing and fabricating probes that not only have the requisite optical performance (resolution, field-of-view), and image acquisition speeds, but also conform to strict design control guidelines in terms of weight, size and other mechanical aspects.

A critical component in any probe development is the scanning mechanism, which can be broadly classified into two categories: proximal and distal[19] (Figure 5). Proximal scanning implies that the scanner is placed at the end of the probe or light guide that is connected at the console of the system, whereas distal refers to the other end of the probe, i.e., the end that is closest to the imaging plane/region. A common configuration for probes incorporating proximal scanning mechanisms typically include a fiber bundle and GRIN (gradient index) lenses for focusing onto the sample.[30–34] Fiber bundles are typically a tightly packed assembly of 10,000 to 100,000 individual optical fibers with an overall diameter that ranges from less than a millimeter to a millimetre.[16,35] The total number of fibers in the coherent bundle determines the total number of pixels in the final image. As the proximal scanner moves the light spot across one end face of the bundle, at any instant of time, only one fiber in the bundle is illuminated which acts both as a point source and as a confocal pinhole. The chief advantage in using fiber bundles as an image guide is that by not having the scanning mechanism as a part of the imaging head, a reduction of the probe size is facilitated. However, the inherent pixilation of the image introduced by the bundle geometry reduces the lateral resolution and since the fibers are tightly packed with very little space in between, optical cross-talk between adjacent fibers is always a possibility. Other proximally scanning probe prototypes that use free-space optics have also been reported.[31,36] Distal scanning schemes primarily involve MEMS (microelectromechanical) scanners[22,37,38] and offer faster imaging speeds and improved image quality over fiber bundle-based probes. For a comprehensive summary of various distal and proximal scanning configurations that have been reported in literature, the reader is referred to Jabbour et al.[19]

At present, there are two commercially available systems for confocal endomicroscopy, namely, the eCLE (confocal endoscope) from Pentax (Tokyo, Japan) and the pCLE (probe-based confocal endomicroscope) from Mauna Kea Technologies (Paris, France). Both systems come equipped with an endomicroscopy image processor and viewing screen and enable visualization of microscopic cellular and vascular patterns. Optiscan, Australia has developed the light source unit and proprietary software for image processing for the Pentax system. The Cellvizio 'miniprobes' that come with Mauna Kea's pCLE system are designed to be passed through the accessory port of a standard white light endoscope whereas Pentax's eCLE imaging head has the confocal endomicroscope incorporated

GRIN: Gradient-index (GRIN) lenses have a gradient profile wherein the refractive index N varies in the direction perpendicular to the optical axis and is expressed as,

$$N = N_0[1 - (k/2)r^2]$$

where N_0 is the base refractive index (at the center of the lens), k is the Gradient Constant, and r is the variable radius.

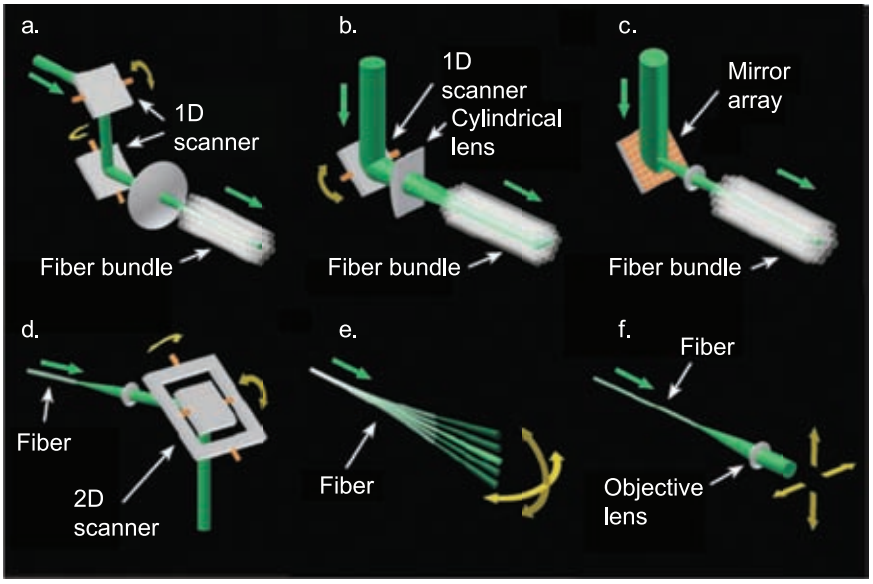

Figure 5: Scanning mechanisms. a. Proximal scanning. Cascaded galvanometer-mounted mirrors scan the excitation beam across the proximal end of a fiber bundle. b. Proximal line scanning with a cylindrical lens. c. Proximal scanning with a spatial light modulator. d. Distal 2D scanning with a miniaturized MEMS mirror. e. Distal fiber tip scanning. f. Distal fiber-objective scanning using an actuated cantilever (not shown).[16]

at its tip and comes equipped with wheels, air, water and suction buttons as well as controls for setting the imaging depth[39–41] (Figure 6). The optical performance specifications for both systems have been enumerated in Table 1, which has been adapted from Paull et al.[41] Both the Pentax as well as the Mauna Kea systems exploit fluorescence contrast and use a blue (488 nm) light source. A large number of studies using these systems have been conducted over the last decade.[9,39,42–44]

In 2003, Sakashita et al. reported the very first demonstration of RCM in vivo via a probe prototype developed by Olympus, Inc.[26] The probe had an imaging rate of 4 frames/s and used a 405 nm laser diode source (Figure 7). A 2008 study conducted by Nakao et al. also involved an RCM catheter prototype and system developed jointly by Mauna Kea Technologies (Paris, France) and Fujinon (Saitama, Japan).[45] Since then, efforts have been channeled into designing compact, miniaturized probes based on reflectance confocal microscopy and SECM for *in vivo* imaging. These probes are commonly deployed through the accessory ports of conventional white light endoscopes and laparoscopic tools. These access ports are typically quite narrow and hence, place restrictions on the size of the probe.

To date, there have been no published reports of clinical *in vivo* studies using probe-based SECM. An early prototype developed by Pitris et al.[46] incorporated two anti-reflection-coated prisms and a grating, the so-called dual-prism grating (DPGRISM) combination to facilitate spectral dispersion and reduce the size of the probe. The underlying principle of a DPGRISM configuration is simple; essentially, the grating (usually one with a high groove density for high diffraction efficiency) changes the direction of the (now dispersed) beam since it has a large diffraction angle. The effect of the two prisms is to steer the beam back to its original direction, i.e., re-orient it so that the illumination from the probe is on-axis

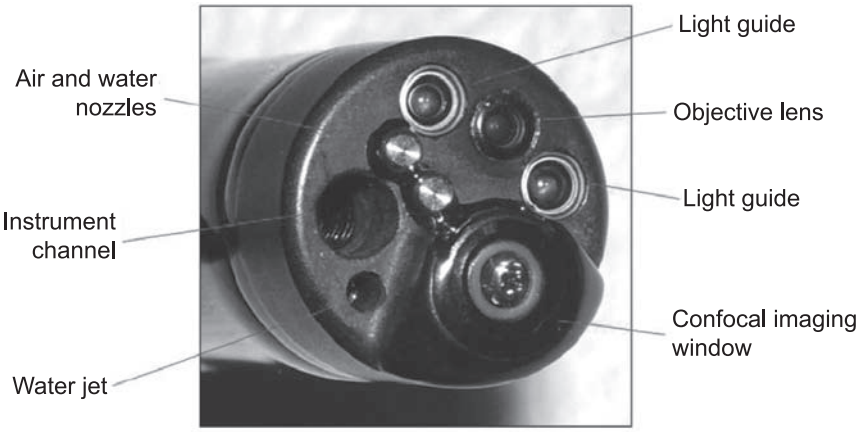

Figure 6: Picture of a confocal scanning head integrated onto the distal tip of a conventional Pentax EC-3870CIFK colonoscope.[40]

Table 1: Specifications of probe-based (pCLE) and standard Endoscope-based Confocal Laser Microscopy (eCLE) and conventional video endoscopy system (adapted from Paull et al.[41]).

	eCLE	pCLE			
	Upper and lower GI	Upper and lower GI	Biliary	Lung	Miniprobe, needle-based
Distal diameter, mm	6.3–12.8	2.6 or 2.7	1	1.4	0.85
Field of view, μm	475	240 or 600	320	600	300
Imaging depth, μm	0–250	70–130	40–70	0–50	30–150
Lateral resolution, μm	0.7	1–3.5	3.5	3.5	3.5
Axial resolution, μm	7	15	15	15	15
Image rate, μm	0.8–1.6	9–12	9–12	9–12	9–12

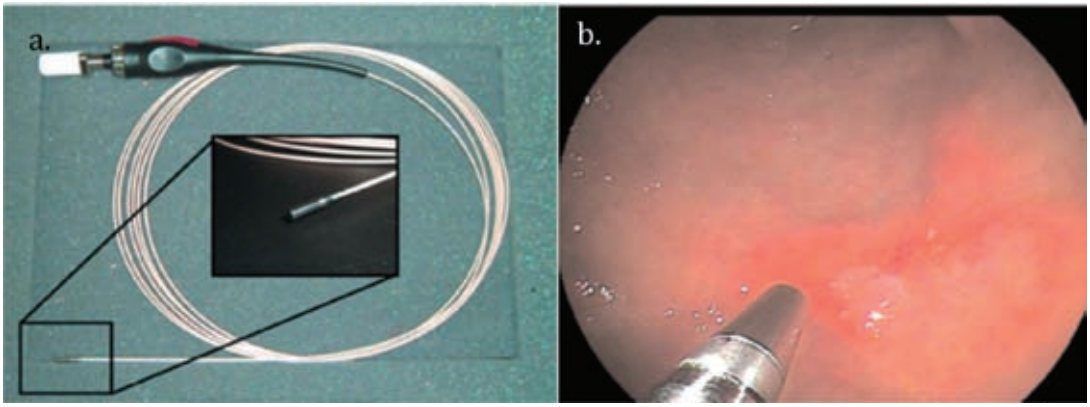

Figure 7: a. Catheter-based reflectance-type laser scanning confocal microscope (Mauna Kea Technologies, Paris, France; Fujinon, Saitama, Japan). b. Laser confocal microscopy examination for early gastric cancer under endoscopy.[26]

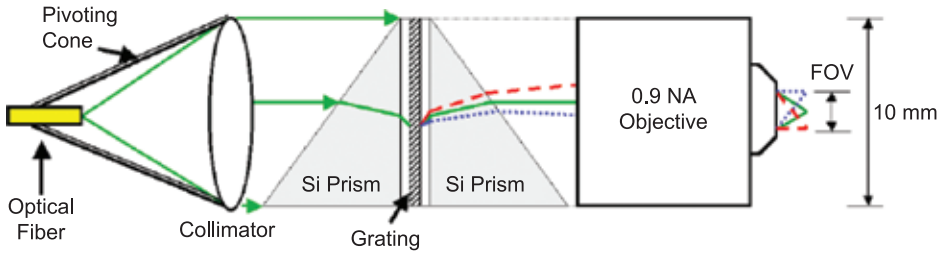

Figure 8: Schematic of the DPGRISM-based SECM probe consisting of a pivoting cone fiber and collimator holder, a dual prism-grating combination, and a modified 0.9 NA water immersion objective.[46]

(Figure 8). Since the illumination emanating from the probe is in a direction orthogonal to the sample plane, the probe can be held perpendicular making it convenient for hand-held applications. This probe had a lateral resolution of 1.1 μm over a 658 nm field-of-view.

Yelin et al[47] demonstrated high-speed comprehensive SECM of large regions by imaging a 2.5 cm-long cylinder of 2.0 cm diameter with a miniature probe prototype in a 2007 paper. Prior to this demonstration of SECM, techniques such as strip mosaicing[48,49] were employed to overcome the inherent 'point-sampling' nature of RCM. In this report, a motor that was 15 mm in diameter, was joined to a metal housing which enclosed a small grating and the focusing aspheric lens. A lens pair preceding the lens-grating assembly (immediately after light from a broadband source was collimated), was incorporated to adjust the position of the focal plane. Helical scanning was accomplished by mounting the probe on a computer-controlled translation stage.

Figure 9 depicts integrated images of a 2.5 cm long lens tissue phantom obtained at five different focal locations. A sample of swine intestine was subsequently imaged but in this case, comprehensive imaging along the entire length of the sample could not be achieved owing to the lack of a centering mechanism for the probe. Confocal imaging involves tight focusing with lenses of high numerical aperture resulting in a small

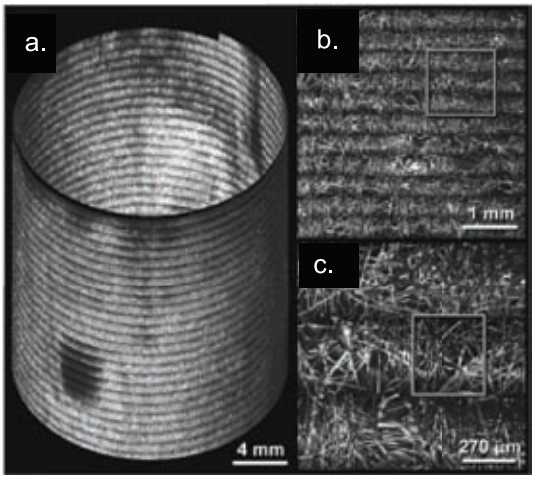

Figure 9: a. Integrated comprehensive SECM image data from a lens tissue paper phantom at multiple focal locations. b. 4.5x magnification of a selected region from the data set. c. 16.7x magnification of the region marked in b.[47]

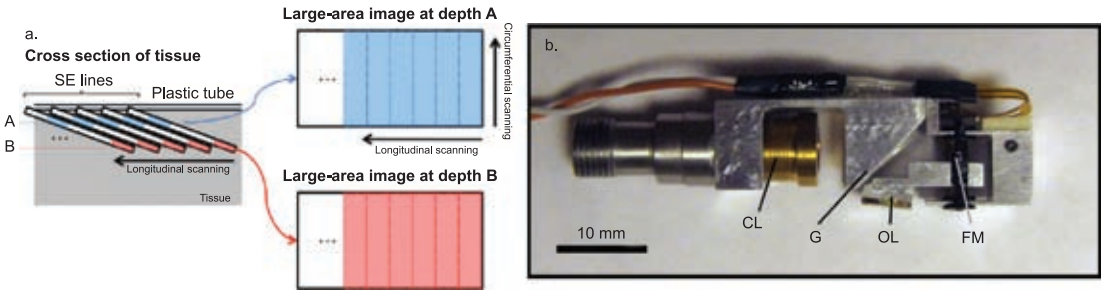

Figure 10: a. Tilted objective approach for obtaining multiple images simultaneously at various depth levels. b. Picture of probe prototype.[50]

depth-of-focus, which becomes a considerable challenge for *in vivo* imaging using SECM endoscopes. Extremely tight tolerances are imposed on the distance between the probe/focusing lens and the plane to be imaged. Any perturbations, in the form of motion or jitter, can result in loss of image information entirely and this has been a major obstruction in translating this technology towards clinical management. To address this issue, in 2011, Kang et al,[50] reported on a novel probe prototype for SECM incorporated with an autofocus mechanism. The design was similar to that reported by Yelin et. al in 2007[47] except for two major modifications: one involved the strategy for obtaining images from different depths simultaneously and this was achieved by tilting the focusing objective lens at an angle of ~5.7 degrees. The field-of-view was measured to be 400 μm. The smallest feature (2.2 μm-wide bars) on an Air Force resolution target was clearly resolved; the axial resolution was 4.4 μm and 10 μm at the center and edges of the field-of-view respectively. The ratio of the field depth to the axial resolution of the probe was calculated to determine the number of distinct depth levels that could be imaged simultaneously. Once the volumetric data was acquired, post processing was done to obtain *en face* confocal images of the sample, which were then stitched together to yield complete images at each depth. Figure 10 depicts the principle used for 3D image acquisition. The second modification was the implementation of adaptive focusing by mounting objective lens on a miniature linear guide and a piezo-electric transducer (PZT) actuator so that the lens could be moved to any location orthogonal to the sample surface. This ensured that the focal plane could be shifted to the desired depth within the sample. The prototype was set up so that it could image from within a cylindrical hollow tract and hence the probe was placed within a transparent cylindrical sheath with the sample wrapped around it. An algorithm was developed to vary the focal location in real-time while the sample was scanned. This involved

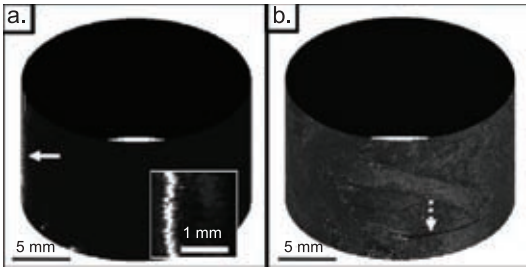

Figure 11: Cylindrical representation of swine small intestine tissue: a. without adaptive focusing (inset depicts magnified image), and b. with adaptive focusing.[50] The dotted arrow points to ~2% of the total imaged area which could not be visualized.

Depth-of-focus: The extent of the region around the image plane in which the image appears to be sharp.

using the high reflectance signal from the sheath to compute the precise location of the objective lens. A signal proportional to the difference between the actual lens position and the target lens position was derived in the form of TTL pulses, which moved the objective to the designated location. Figure 11 depicts images of a swine intestine sample obtained with and without the adaptive focusing mechanism and the lack of image information in the latter can be clearly noted.

In 2012, Kang et al. demonstrated the assembly of a custom, water-immersion molded, aspheric objective lens with an overall diameter of 3 mm and a miniature diffraction grating along with the requisite collimation optics, which consisted of a spacer and a GRIN lens, enclosed within a stainless steel housing.[51] The entire assembly was placed within a transparent sheath that had an index of refraction similar to tissue (~1.338). The light guide for the probe was a dual-clad optical fiber. The probe was capable of confocally imaging a 5 cm-long segment of the esophagus (representative of the entire distal esophagus) within 4 minutes when used with a wavelength-swept source with a 100 kHz sweep rate. The overall footprint of this probe was small enough to facilitate *in vivo* use for the GI tract with an outer diameter of 5.85 mm and a length of 25 mm.

Designing any endoscopic imaging probe, in general, is becoming increasingly complex owing to stringent size restrictions and a constant push to improve imaging quality. Commercially available ray-tracing software such as Zemax or Code V are routinely used for evaluating the optical design while mechanical layouts are specified with SolidWorks and AutoCad. A scheme that can be exploited for SECM probe development is one that is currently in use for balloon catheters for Optical Frequency Domain Imaging (OFDI), which is a non-contact, interferometric ranging technique derived from optical coherence tomography (OCT).[52–54] Conventional OCT[55–60] is based on a Michelson interferometer configuration and is performed in the time domain by mechanically translating the reference mirror. OCT obtains structural information by using coherence gating and is used for imaging at high resolutions within scattering tissue. However, image acquisition speeds are limited since each point in the image is obtained by sampling sequentially. OFDI overcomes this limitation by using a monochromatic wavelength-swept source (described later) and performs depth ranging by maintaining a constant reference arm while varying the wavelength rapidly. Hence, all points at a certain depth are sampled simultaneously leading to improved image rates (100-fold faster than time-domain OCT) and higher detection sensitivities.[54,61,62] By sweeping the wavelength, spectral interference is generated, which is Fourier, transformed to form an image. Typical resolutions of cross-sectional images are 30 (H) × 30 (W) × 10 μm (D) and penetration depths range from 100 to 300 μm. OFDI probes combine rotational and translational motion so that the region of interest can be scanned helically. OFDI catheters consist of an inner cable, which contains the distal optics and the optical fiber. This inner cable is enclosed within a transparent outer sheath or balloon and is coupled to the console via an optical rotary junction (Figure 12a). The rotary junction, in conjunction with a pullback device, can rotate the probe at speeds up to 4 revolutions/s and the pullback tray translates the probe at ~10 μm per second (Figure 12b).[52] OFDI balloon catheters have been successfully implemented for numerous studies (over a 1000 human subjects). This scheme has the potential to be extended to SECM for the screening and surveillance of regions such as the GI tract.

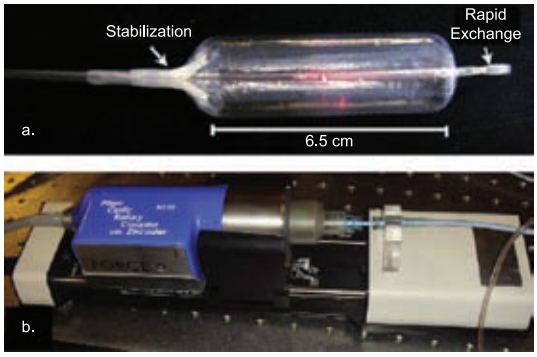

Figure 12: a. Balloon catheter with a 1 mm-diameter inner optical core. The balloon inflates to dilate the esophagus and center the inner optical core. b. Optical rotary junction mounted on a pullback tray and connected to the proximal portion of the imaging catheter.[52]

3.2 *Speckle and double-clad fibers*

SECM (or any embodiment of RCM which involves light from a laser) is essentially a coherent imaging technique. Speckle is a source of artifacts in images obtained with coherent light. Speckle noise not only degrades image quality but also decreases the effective resolution. Speckle results from the interference of randomly phased reflections, which occur from the microscopic surface irregularities present on surfaces, which act as sub-resolution scatterers and appears as a random, deterministic, micro-scale granular intensity pattern. The intensity fluctuations originate from the interference of randomly phased reflection from illuminated surface facets. As stated by Goodman,[63,64] "…speckle appears when a signal is composed of a multitude of independently phased additive complex components that may have random directions and known or random amplitudes. When these components add together, as dictated by their phases, the resultant constitutes a 'random walk'". Two parameters that are often employed to characterize the extent of speckles present in images are the speckle contrast (C) and the signal-to-noise (SNR) ratio of the pattern. The contrast measures the strength of the intensity fluctuations in the speckle pattern (σ_I) compared to the average intensity ($\bar{I}$) and is defined as the ratio of the rms fluctuation of the granularity to its mean intensity, i.e.,

$$C = \sigma_I/\bar{I} \tag{9}$$

The signal to noise ratio is the reciprocal of the contrast. For a fully developed speckle pattern or pure diffuse scattering, i.e., speckles with a vanishing specular field component, which occur typically with very rough surfaces and a monochromatic, completely coherent light source, the speckle contrast (and hence SNR) is unity.

In conventional confocal microscopy, there are a few techniques for speckle reduction such as the use of multiple lasers of different wavelengths,[65] or rotating diffuser[66] or by illuminating the image field with a mix of varying beam angles.[67] Conventional table-top confocal microscopes address this issue by using a slightly larger diameter for the detection aperture than for the illumination pinhole. Essentially, the speckle pattern in an image is 'averaged out' by superimposing multiple speckle patterns at varying projection angles and adding them together. When the detection aperture is enlarged, speckles at different projection angles are allowed to propagate. With the development of dual-clad or double-clad optical fibers, this concept is readily translated to fiber-based confocal endoscopy.

Double-clad fibers (DCFs) were originally developed for fiber laser systems[68] and differ from conventional optical fibers by the inclusion of an additional cladding region. Figure 13 depicts the typical profile of a DCF as compared to conventional single and multimode fibers. A DCF consists of two concentric cladding regions around a single core. The inner cladding acts as a multi-mode waveguide and a channel additional to the central core. The backscattered light from the sample plane excites multiple orthogonal modes within the inner cladding of the DCF; each of these modes are then detected independently at the detector, leading to lower speckle contrast of the final image. This combination of a single-mode illumination (of the sample) and multi-mode detection, is also referred to as a partially coherent scheme. Figure 14 depicts images of lens tissue paper obtained via SECM in a fully coherent and a partially coherent scheme, clearly highlighting the speckle reduction for the latter.

In 2004, Yelin et al. reported the use of a commercially available double-clad fiber (SM900, Fibercore Ltd.) for spectrally encoded endoscopy,[69–71] which is another form of endoscopy using spectral encoding with interferometric detection techniques.

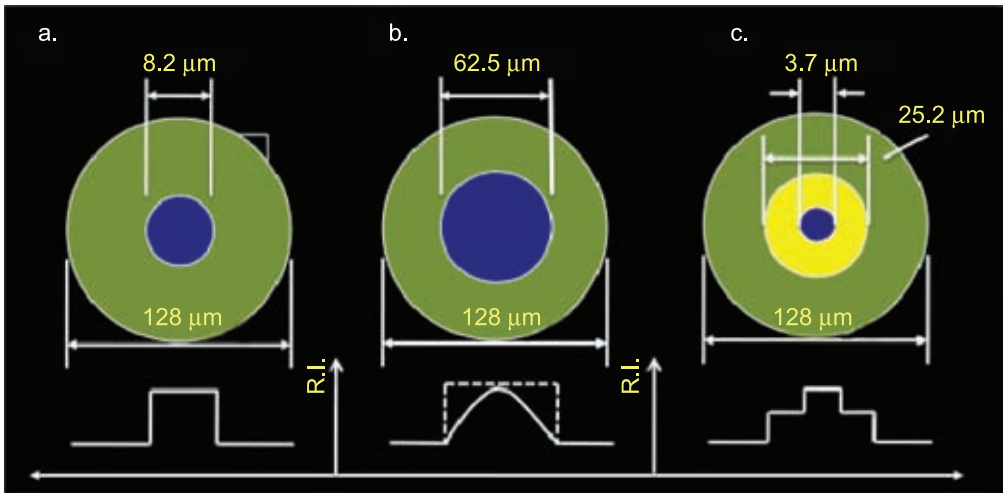

Figure 13: Schematic of cross-sectional and refractive index (R.I.) profiles of a. single-mode fiber, b. multimode fiber, and c. double-clad fiber.

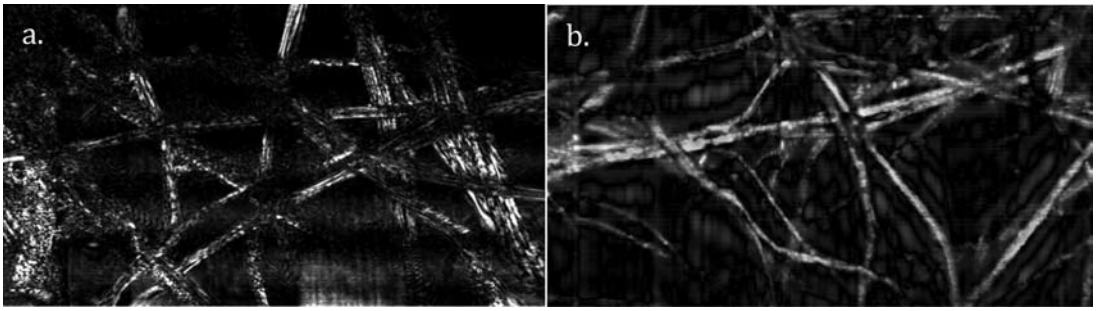

Figure 14: SECM images of lens tissue obtained using a. single-mode fiber and b. double-clad fiber.[72]

Figure 15 illustrates the results obtained by them both experimentally as well as numerically. By switching to the DCF, they were able to reduce the speckle contrast by nearly a factor of 8. Since the detection aperture, which was now the DCF inner cladding, was larger, more light could be collected leading to a significant increase of the optical throughput (about 32 times stronger than the single mode fiber case) and increased depth-of-field. Opening up the detection aperture comes with the penalty of loss in resolution, however, with a careful choice of the aperture diameter, a reasonable trade-off can be achieved.[73] This is especially relevant for clinical applications where slightly lower resolutions may not be as much of a hindrance as speckle artifacts, which can easily cause misinterpretations of the pathological features present in an image.

More recent research on double-clad fiber-based endoscopy has involved the design and fabrication of DCF couplers by a variety of different techniques,[74] which greatly improve the robustness of SECM setups by eliminating bulk optical components such as beamsplitters and collimating lenses and their associated reflection losses. Lemire-Renaud et al. modified their achromatic DCF coupler by tapering/post-processing the imaging arm so that they could have greater control over the ratio of the illumination and detection aperture diameters[75] (Figure 16). In 2012, Kang et al. reported the demonstration of a high-speed esophageal endoscopic probe with a DCF that shows potential for in vivo use.[76]

3.3 *Light sources*

As mentioned earlier, SECM systems use either a broadband light source or a wavelength-swept laser. The broadband light is obtained either from a multiplexed SLED source or a supercontinuum

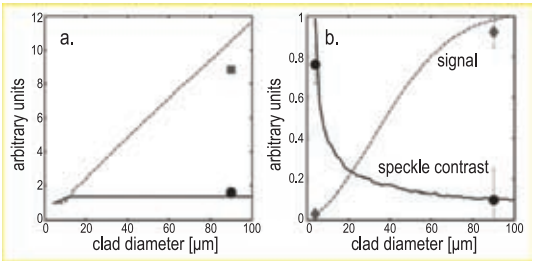

Figure 15: Optical performance of a partially coherent scheme: a. normalized transverse (solid) and axial (dashed) spot sizes as a function of the inner cladding diameter. b. Speckle contrast and normalized total signal intensity. The solid dots and squares represent simulation results.[69]

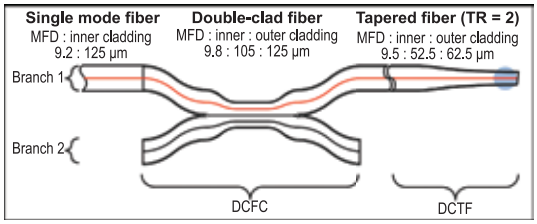

Figure 16: Schematic of a double-clad fiber coupler with a tapered end; the gray region represents a high-index gel drop to minimize back reflections.[75]

source. When a narrow-band pulse of light propagates within a suitable optical medium due to a plethora of nonlinear effects, it undergoes extreme broadening via a process known as supercontinuum generation (SCG). Alfano and Shapiro first observed the spectral broadening of a narrow-band pulse as a result of a variety of nonlinear interactions in bulk BK7 glass in 1970.[77] This phenomenon regained interest in the late 70s when Stolen and Lin demonstrated continuum generation in optical fibers.[78] Research in SCG received a boost with the advent of a new class of optical fiber waveguides, known as photonic crystal fibers (PCFs), in the late 1990s.[79] PCFs possess unique cross-sectional morphologies, which give rise to a variety of novel propagation characteristics including enhanced modal confinement and therefore higher effective nonlinearity, single mode behavior over broad wavelength ranges ('endlessly single mode') and engineerable group velocity dispersion. Researchers have exploited supercontinuum generation as broad, spatially coherent, high brightness, tunable spectral sources for fields as diverse as ultrafast spectroscopy, pulse compression, optical metrology, and optical coherence tomography.[80–82] The generation of broadband spectra in the telecommunications window in the context of the development of wavelength division multiplexed systems has direct implications for SECM. Attributes like the high spectral density and brightness make SCG an ideal candidate for a source for SECM.

A wavelength-swept laser was first used by Boudoux et al.[83] for imaging human skin in vivo using SECM at high speeds (30 frames/s). A wavelength-swept source is essentially a tunable light source, emitting one wavelength at a time, swept rapidly over a broad spectral range. These lasers provide high-power polarized light, narrow linewidth, broad wavelength tuning ranges, fast repetition rates and yet are compact and environmentally stable. SECM requires that the output of these lasers possess narrow instantaneous linewidths to

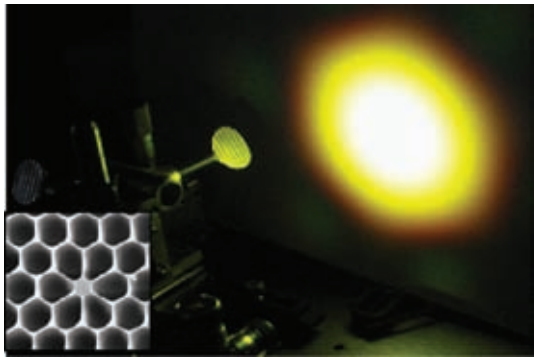

Figure 17: High-intensity, supercontinuum generation light emitted by the injection of 100 fs pulses at 800 nm into a photonic crystal fiber (inset: magnified fiber cross-section).

preserve spatial resolution, have high repetition rate for fast imaging speeds and scan linearly over a broad spectral range to maintain a large field of view. The reflectivity of biological tissue is of the order of 10^{-4}, i.e., the back-reflected signal intensity is extremely weak, and hence, the total optical power of the laser as well as the background suppression ratio should be sufficiently high.

A widely used gain medium for wavelength swept sources is a semiconductor optical amplifier (SOA) as the flexibility of semiconductors in making heterogeneous structures yields a wide choice of gain center wavelengths.[84,85] Typical materials for SOAs are III-V compound semiconductors such as GaAs/$Al_xGa_{(1-x)}As$ (for center wavelengths ranging from 0.75 μm to 0.9 μm) and $In_{(1-x)}Ga_xAs_{(1-y)}P_y$/InP (for center wavelengths ranging from 1.1 μm to 1.6 μm). An SOA offers high gain with broad bandwidth, which gives great flexibility in choosing a filter and cavity configuration for wide and fast tunability. Also, the gain response time of an SOA is much shorter than that of other widely used gain media (such as a Ti:Sapphire crystal) and rare-earth doped fibers. This facilitates fast sweep operations since short gain response times minimize the intensity noise of the laser output. For SECM, an instantaneous a linewidth of 10 GHz (<0.06 nm) or so is narrow enough to provide transverse resolutions of a few micrometers. Scanning filters based on rotating grating-mirrors and Fabry-Pérot etalons have been implemented in swept laser sources[56,68] but the tuning frequencies have been restricted to 1 kHz which is insufficient for frame rates exceeding video rates. In 2003, Yun et al. developed a novel wavelength scanning filter comprising a polygonal scanner, diffraction grating, and an afocal telescope. Their intracavity, narrowband, polygon-based, wavelength scanning filter achieved simultaneously, a high sweep rate, a wide tuning range and a narrow laser linewidth.

The description for the polygonal scanner has been adapted from Yun et al.[86] The telescope is constructed with two mirrors in an infinite-conjugates configuration with the grating at the front focal plane of lens 1 and the polygon spin axis at the back focal plane of lens 2 (Figure 18). The telescope converts diverging angular dispersion from the grating into converging angular dispersion after the second lens, and it controls the imaged beam size and convergence angle at the polygon. The polygon reflects back only the spectral components within a narrow resolution band normal to the front mirror facet of the polygon. The reflected component is dispersed again as it falls on the diffraction grating for the second time and is received by the fiber. The orientation of the beam's incidence angle and the rotation direction of the polygonal mirror determine the direction of wavelength tuning.

The center wavelength of the tuning range of the filter is given by

$$\lambda_0 = g(\sin\alpha_0 + \sin\beta_0), \tag{10}$$

where α is the incidence angle of the beam, β_0 is the angle between the optical axis of the telescope and the grating normal, and g is the grating pitch. The tuning range of the filter is fundamentally limited by the finite numerical aperture of the first lens, which is given by,

$$\Delta\beta = (D_1 - W\cos\beta_0/\cos\alpha)/F_1, \tag{11}$$

where D_1 and F_1 are the lens' diameter and focal length respectively and W is the $1/e^2$ width of the beam at the collimator. From the acceptance angle, the filter tuning range is given by,

$$\Delta\lambda = g\cos\beta_0\Delta\beta \tag{12}$$

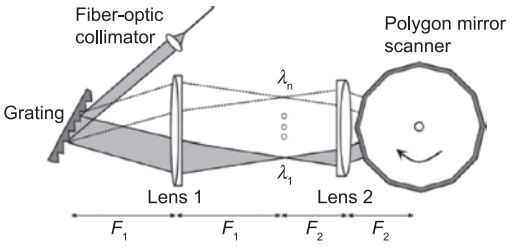

Figure 18: Schematic of the high speed, wavelength scanning filter.[86]

Afocal telescope: An optical telescope where both the light entering the system as well as the image formed is at infinity. An afocal optical system has no focus, i.e., is a system that produces no net convergence or divergence of the entering beam. An afocal system can be created with a pair of optical elements where the distance between the elements is equal to the sum of each element's focal length ($d = f_1 + f_2$).

One major advantage of the polygon filter is the flexibility in varying the tuning speed, range, resolution or wavelength by simply controlling the rotational speed, grating angle or the magnification of the telescope. The polygon-based filter was incorporated into an extended-cavity semiconductor laser via a Faraday circulator. The gain medium was a SOA (Phillips CQF 882/e), and the laser output was obtained through the 90% port of a fiber-optic fused coupler.

Esophagogastroduodenoscopy (EGD): A diagnostic endoscopic procedure that visualizes the upper part of the gastrointestinal tract up to the duodenum.

4 Medical Applications of SECM

The very first demonstration of RCM *in vivo*[26] was a study to compare images of resected colorectal lesions obtained via standard histology and confocal microscopy. In this study, an Olympus endomicroscope probe was used without any dyes or other contrast agents. Since then, a multitude of reports of reflectance confocal microscopy as a diagnostic modality have been published.[87–91] The same year, a fiber-optic confocal reflectance microscope based on a 30,000-element fiber bundle was also developed to visualize precancerous cervical conditions in 18 patients.[92] With the probe, the authors were able to observe an enlargement in nuclear size with respect to the cell, which is a known hallmark of cervical precancer. The first human study to diagnose cancer of the GI tract using RCM was done a few years later[45] where a 685 nm diode was incorporated in a fiber bundle probe, which had to be placed in contact with the tissue surface. The probe was 6.9 mm in diameter and 250 mm long. The objective lens was placed in contact with each specimen, the focus was 30 μm from the objective lens and the resolution was less than 1 μm. The results of this study, although not robust enough for a complete diagnosis (malignant lesions could not be distinguished from benign lesions in all cases), were encouraging in that irregular nuclei were clearly visualized in gastric and colonic cancer specimens.

Dysplasia: The enlargement of an organ or tissue by the proliferation of cells of an abnormal type.

The first study which highlighted SECM's potential for clinical utility was reported in 2010[93] in which the goal was to demonstrate large-area SECM in upper GI tissues and to determine whether the images contain microstructural information that is useful for pathologic diagnosis. Fifty biopsy samples from 36 patients undergoing routine esophagogastroduodenoscopy (EGD) were imaged by SECM, in their entirety, immediately after their removal.The setup was a benchtop system with a water immersion objective lens (focal length = 5.3 mm), which was used to generate a single-scan field length of 180 μm along the spectrally encoded axis of the image. For obtaining multiple depth scans, a piezoelectric transducer actuator changed the position of the objective lens. The transverse resolution was measured to be 2 μm and the axial resolution was 10 μm. The image dimension varied from 2 × 1 mm (4000 × 2000 pixels) to 5 × 3.6 mm (10,000 × 7200 pixels). The total depth imaged ranged between 120 and 150 μm. Figure 19 depicts SECM images of a biopsy sample taken from a female patient with a history of dysplasia. What was notable in this study was that a probe prototype designed for this benchtop system was capable of imaging a 2.5 cm-long section of a cylindrical region of 2.0 cm-diameter.[47] The unique wavelength-to-spatial-coordinate mapping aspect of SECM contributed to the improvement in the imaging speed over previous reflectance confocal techniques.

In another experiment involving biopsy samples taken from a patient with high-grade dysplasia and Barrett's esophagus, the SECM benchtop system was combined through a fold mirror with an OFDI system to result in a multimodal imaging platform that offered two different resolution scales (architectural and morphological

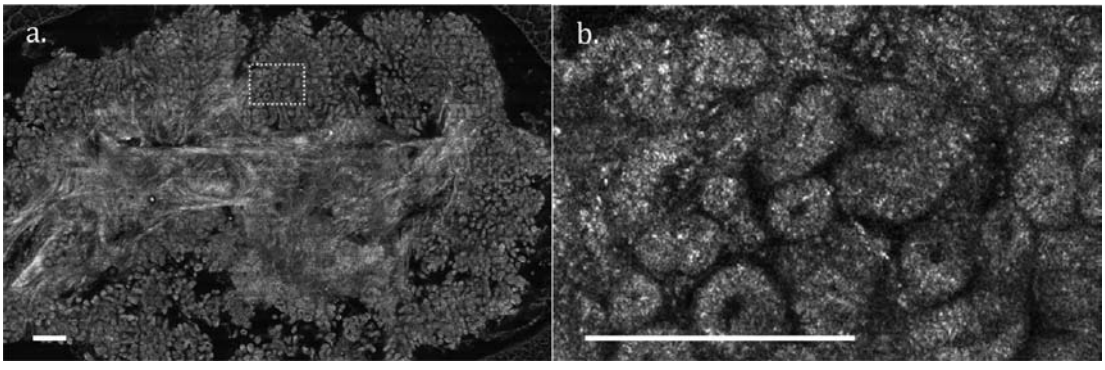

Figure 19: SECM images of a fundic gland polyp stained with 0.6% acetic acid. a. SECM image shows tightly packed glands. b. High magnification image of boxed region in a. Scale bars represent 250 μm.[93]

information from OFDI and transverse cellular features from SECM) as well as display formats.[94] This combined system provided co-registered *en face* images where gastric cardia-type mucosa could be clearly distinguished from normal squamous mucosa. The registration error was measured to be around 50 μm by calculating the location of the maximum of the two-dimensional cross-correlation of the two images. Overall, preliminary images demonstrated good spatial correspondence between the two imaging modalities.

Opthalmology is a field that has benefitted greatly from noninvasive optical imaging techniques, most notably, OCT.[95–99] In 2010, Tao et al. reported the implementation of a spectrally encoded confocal scanning laser opthalmoscope (SECSLO) for fundus imaging.[100,101] High-resolution retinovitreal imaging by confocal scanning laser ophthalmoscopy (CSLO) has been an existing technology for some time. A modified version of CSLO, wherein, a focused light and not a spot, is raster scanned over the retina, has also been reported However, CSLO designs typically involve bulk optics which introduces complexity in the systems. The setup used by Tao et al.[101] comprised of a superluminescent diode (SLED) with a 49 nm bandwidth as their illumination source and relayed this through a high groove density diffraction grating, a single-axis galvanometric scanner, a relay lens, and an aspheric ophthalmic lens. Detection was done by a custom spectrometer based on a 1024 pixel line-scan CCD array with a line rate of 52 kHz. The system is depicted in Figure 20a. *In vivo* human fundus imaging was achieved at 10 kHz line rate.

In 2011, SECM was used for a pilot study for the diagnosis of eosinophilic esophagitis *ex vivo*.[91] Eosinophilic esophagitis (EoE) is an inflammatory disease that afflicts both the adult as well as the pediatric population and is characterized by the presence of eosinophils within the esophageal squamous epithelium.[102–112] The management of EoE entails adherence to a controlled dietary regiment accompanied by periodic monitoring of the esophagus.[113] The monitoring involves repeat upper endoscopies with biopsy under sedation, which is expensive and tedious. Since SECM is capable of comprehensively imaging large sections of the esophagus at high, cellular-level resolutions, it has the potential to serve as an accurate diagnostic tool for EoE. For the pilot study reported by Yoo et al., 43 biopsy samples were extracted from 35 pediatric patients at the Massachusetts General Hospital. The imaging was done immediately after the samples were obtained. A bench-top SECM system was employed for imaging the biopsy samples. In order to improve the signal to noise ratio and reduce speckle artifacts, a single-mode illumination and multi-mode/partially coherent detection scheme (described earlier in this article) was used. The transverse axial (depth) resolutions of the bench-top SECM system were 2.3 μm and 9.7 μm respectively and the total depth range was about 200 μm.

Eosinophils: White blood cells that form an essential component of the immune system.

The diagnostic criteria for EoE requires an eosinophil count from the proximal, middle, and distal regions of the esophagus; a biopsy with an eosinophil count higher than 15 per high power field (HPF = 400x) under a microscope is considered to be a positive diagnosis of EoE.[102] The authors were able to visualize highly reflecting dots within the epithelium, which they identified as eosinophils (Figure 21). They hypothesized that eosinophils can be visualized with high-contrast by SECM owing to its large size and high refractive index gradient associated with the granules present in the cytoplasm which leads to increased backscattering. The results of the study

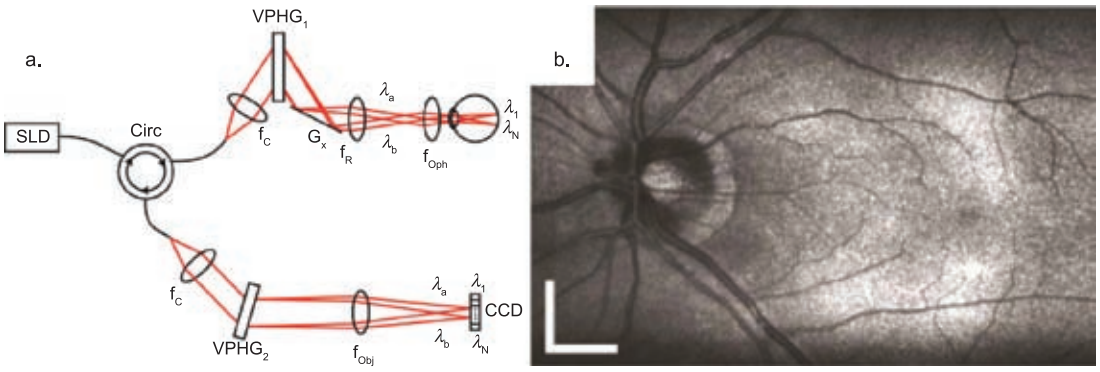

Figure 20: a. Fiber-based spectrally encoded ophthalmoscope. CCD, linear CCD array; f, focal length of collimating, relay, and focusing elements; G, galvanometer; VPHG, grating. b. 7 x 5 mm (lateral x spectral) image of *in vivo* human fundus.[101]

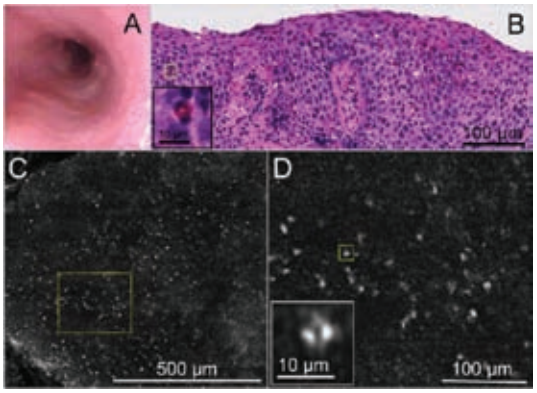

Figure 21: Images obtained from an 11-year-old male patient with eosinophilic esophagitis. A. Videoendoscopy image. B. Histopathology demonstrating an abundance of eosinophils within the squamous epithelium. C. SECM image obtained 50 µm below the surface; inset shows a bilobed eosinophil nucleus. D. Higher magnification view of the yellow dotted box in C; inset shows a bilobed eosinophil nucleus.[91]

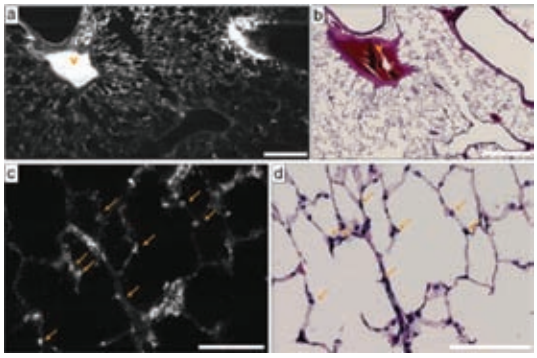

Figure 22: SECM and histology images of PBS-immersed fixed rat lung slice. a. En-face SECM image 70 µm under tissue surface. b. Corresponding histology where V indicates a vessel; scalebar = 500 µm. c. SECM image at higher magnification, where arrows indicate alveolar type II pneumocytes. d. Corresponding histology; scalebar = 100 µm.[114]

demonstrated that RCM, in general, is capable of visualizing and counting the number of intraepithelial eosinophils as well as characterizing other key features such as eosinophil abscess and basal cell hyperplasia.

SECM has also been utilized for pulmonary imaging. Unglert et al. reported comparison studies of three major optical reflectance techniques, namely, SECM, OCT and FFOCM (full-field, optical coherence microscopy) for imaging alveolar structures of the peripheral lung.[114] Fresh lungs were excised from three adult rats, inflated at 20 cm H_2O pressure through a gravity feed system and subsequently air-dried. Cylindrical sections that were 1–2 mm thick were obtained from the air-dried lungs and immersed into PBS for imaging. The higher refractive index contrast between air and tissue, which leads to increased refraction, resulted in increasedimaging depths for liquid-filled (PBS in this case) as opposed toair-filled alveoli. The imaging depths varied from 100–150 µm depending on the specific structure (alveoli versus blood vessels and their surrounding collagen matrix).

Of late, there has been a push to develop optical reflectance techniques as an imaging modality to complement existing imaging and diagnostic tools for pulmonary imaging. For instance, histology and micro-computed tomography (Micro CT), whichis a non-destructive imaging technology where x-rays are used to generate 2D slices of the sample for generating a 3D model to study morphological properties,are accepted tools for pulmonary imaging.[115] In Micro CT, the sample thickness is directly correlated to the resolution (typically, ~9 µm for an 8 mm-thick sample and 400 nm for a 200 nm thick sample) and this hinders the wide application of Micro CT for lung imaging within whole animal models. Pulmonary motion makes Micro CT challenging for in vivo scenarios, an issue that is well addressed by optical reflectance techniques which image at video rates and thus have very short acquisition times that greatly reduce motion-related artifacts.

The SECM study was carried out on a benchtop system based on a wavelength-swept laser source and the focusing objective was an Olympus 60X water immersion objective with an NA of 1.3 and a focal length of 3 mm. The transverse and axial resolutions were 1.3 µm and 2.4 µm respectively and the length of the spectrally encoded line was 120 µm. A $2 \times 2 \times 0.2$ mm volume was imaged in about 30 minutes. The regions of airway epithelium, vessel endothelium, blood, and aggregations of cell nuclei generate larger SECM signals and are hence, brighter. SECM was able to visualize Type II pneumocytes, which were matched to the corresponding histology images (Figure 22).

5 Outlook and Future Directions

SECM is a relatively new biomedical imaging technique and development of probes for use *in situ* as well as faster systems for rapid data acquisition is currently underway. Recent efforts have also been made to come up with schemes that do away with mechanical scanning entirely. In 2009, Tsia et al reported a novel implementation of the spectral encoding concept, by illuminating the

Full-field, optical coherence microscopy (FFOCM): Imaging based on coherence gating in a Linnik interferometer configuration. En face images are reconstructed via a phase-shifting algorithm.

Pulmonary alveoli: Anatomical structure in the form of a hollow cavity that forms the terminal ends of the mammalian respiratory tree and is the site where gas exchange takes place.

Type II pneumocytes: Large, roughly cuboidal cells that aid in the maintenance of alveoli.

sample with a 'spectral shower'.[116] They called it 'SECOMM' (spectral shower encoded confocal microscopy). In SECOMM, both scan directions were encoded in wavelength by using a 2D spatial disperser. This disperser, also known as a virtually imaged phased array (VIPA), was comprised of a diffraction grating and a tilted Fabry-Perot cavity. In addition to imaging, the authors demonstrated the added functionality of laser ablation surgery through the incorporation of a cw external-cavity frequency tunable diode laser (1520 nm–1570 nm) into their system. Since each wavelength was mapped to a distinct spatial coordinate on the sample plane, the ablation beam could be steered to any desired location within the imaging field by simple tuning the wavelength. The authors propose SECOMM as a versatile tool for performing high-precision surgeries (such as tumor removal and Parkinson's disease treatment procedures in the deep brain) *in situ* and visualizing the changes and processes taking place simultaneously.

Spectral encoding has also been applied outside of tissue imaging. Golan et al.[117] reported the construction of a flow cytometer with subcellular lateral resolution based on SECM. Conventional fluorescence microscopy techniques are often ineffective for rapid blood flows whereas faster imaging modalities such as ultrasound lack the resolution to visualize subcellular features. The spectrally encoded flow cytometer did not require any mechanical scanning since one dimension was encoded in wavelength whereas the other was encoded in time. This concept was demonstrated by creating a steady laminar flow of diluted blood in a polymethyl methacrylate (PMMA) channel with a 0.55 mm × 0.55 mm cross-section. The temporal resolution of the cytometer enabled velocity measurements of unstained blood cells *in vitro*.

A recent publication described a novel, tethered optomechanical capsule endoscope for performing high speed OFDI *in vivo*.[118] All of the distal imaging optics (ferrule, spacer, focusing lens and a dispersive prism) was enclosed within the capsule, which was tethered to an optical rotary junction. This 'imaging pill', in addition to performing high resolution imaging of the entire esophagus in patients, also was found to cause considerably less discomfort than an endoscopic examination. It is not hard to envisiona similar probe embodiment for SECM since the miniature optics required for performing SECM are not too different from OFDI and can be easily accommodated within the capsule. In addition, as was observed in the OFDI tethered capsule study, the luminal organs constrict around the capsule and hence, maintaining the device's focus on the tissue may not be as tricky as with a conventional balloon catheter.

In summary, SECM is a newly developed biomedical imaging tool that allows virtual histology of tissue during ongoing endoscopy. This minimally invasive optical imaging technique allows unique visualization of living cells and cellular structures at and below epithelial surfaces *in vivo* and bridges the interface between endoscopy and histology. Several published studies have already been published which demonstrate the diagnostic spectrum and accuracy of SECM. There is plenty of scope for further development including, but not restricted, to reducing probe sizes for use in less accessible and more complex organ systems while maintaining a high standard of optical performance, increasing the penetration depth of imaging as also pushing the limits of imaging speeds.

Received 14 February 2013.

References

1. Falk, G.W., Rice, T.W., Goldblum, J.R. & Richter, J.E. "Jumbo biopsy forceps protocol still misses unsuspected cancer in Barrett's esophagus with high-grade dysplasia". *Gastrointest Endosc* **49**, 170–176 (1999).
2. histology.leeds.sc.uk.
3. Minsky, M. Microscopy Apparatus. (USA, 1961).
4. Minsky, M. "Memoir on Inventing the Confocal Scanning Microscopy". *Scanning* **10**, 128–138 (1988).
5. Wilson, T. *Confocal Microscopy*, (Academic Press, San, Diego, Calif., 1990).
6. Wilson, T. & Hewlett, S.J. "Superresolution in confocal scanning microscopy". *Optics letters* **16**, 1062–1064 (1991).
7. Georgakoudi, I. & Feld, M.S. "The combined use of fluorescence, reflectance, and light-scattering spectroscopy for evaluating dysplasia in Barrett's esophagus". *Gastrointest Endosc Clin N Am* **14**, 519–537, ix (2004).
8. Lambert, R. "Can endoscopic autofluorescence imaging improve the detection of neoplasia in patients with Barrett's esophagus?". *Nat Clin Pract Gastroenterol Hepatol* **2**, 570–571 (2005).
9. Polglase, A.L., McLaren, W.J., Skinner, S.A., Kiesslich, R., Neurath, M.F. & Delaney, P.M. "A fluorescence confocal endomicroscope for in vivo microscopy of the upper- and the lower-GI tract". *Gastrointest Endosc* **62**, 686–695 (2005).
10. Thiberville, L., Salaun, M., Lachkar, S., Dominique, S., Moreno-Swirc, S., Vever-Bizet, C. & Bourg-Heckly, G. "Confocal fluorescence endomicroscopy of the human airways". *Proc Am Thorac Soc* **6**, 444–449 (2009).
11. Arifler, D., Guillaud, M., Carraro, A., Malpica, A., Follen, M. & Richards-Kortum, R. "Light scattering from normal and dysplastic cervical cells at different epithelial

Flow cytometer: A laser-based technique for cell-counting, sorting, biomarker detection and protein engineering, by suspending cells in a stream of fluid and passing them by an electronic detection apparatus.

depths: finite-difference time-domain modeling with a perfectly matched layer boundary condition". *Journal of biomedical optics* **8**, 484–494 (2003).

12. Carlson, K., Pavlova, I., Collier, T., Descour, M., Follen, M. & Richards-Kortum, R. "Confocal microscopy: imaging cervical precancerous lesions". *Gynecol Oncol* **99**, S84–88 (2005).
13. Kiesslich, R., Gossner, L., Goetz, M., Dahlmann, A., Vieth, M., Stolte, M., Hoffman, A., Jung, M., Nafe, B., Galle, P.R. & Neurath, M.F. "In vivo histology of Barrett's esophagus and associated neoplasia by confocal laser endomicroscopy". *Clin Gastroenterol Hepatol* **4**, 979–987 (2006).
14. Muldoon, T.J., Anandasabapathy, S., Maru, D. & Richards-Kortum, R. "High-resolution imaging in Barrett's esophagus: a novel, low-cost endoscopic microscope". *Gastrointest Endosc* **68**, 737–744 (2008).
15. Pohl, H., Rosch, T., Vieth, M., Koch, M., Becker, V., Anders, M., Khalifa, A.C. & Meining, A. "Miniprobe confocal laser microscopy for the detection of invisible neoplasia in patients with Barrett's oesophagus". *Gut* **57**, 1648–1653 (2008).
16. Flusberg, B.A., Cocker, E.D., Piyawattanametha, W., Jung, J.C., Cheung, E.L. & Schnitzer, M.J. "Fiber-optic fluorescence imaging". *Nature methods* **2**, 941–950 (2005).
17. Mehta, A.D., Jung, J.C., Flusberg, B.A. & Schnitzer, M.J. "Fiber optic in vivo imaging in the mammalian nervous system". *Current opinion in neurobiology* **14**, 617–628 (2004).
18. Rajadhyaksha, M., Anderson, R.R. & Webb, R.H. "Video-rate confocal scanning laser microscope for imaging human tissues in vivo". *Appl Opt* **38**, 2105–2115 (1999).
19. Jabbour, J.M., Saldua, M.A., Bixler, J.N. & Maitland, K.C. "Confocal endomicroscopy: instrumentation and medical applications". *Ann Biomed Eng* **40**, 378–397 (2012).
20. Tearney, G.J., Webb, R.H. & Bouma, B.E. "Spectrally encoded confocal microscopy". *Optics letters* **23**, 1152–1154 (1998).
21. Boudoux, C. Massachusetts Institute of Technology (2007).
22. Dickensheets, D.L. & Kino, G.S. "Micromachined scanning confocal optical microscope". *Optics letters* **21**, 764–766 (1996).
23. Carlson, K., Chidley, M., Sung, K.B., Descour, M., Gillenwater, A., Follen, M. & Richards-Kortum, R. "In vivo fiber-optic confocal reflectance microscope with an injection-molded plastic miniature objective lens". *Appl Opt* **44**, 1792–1797 (2005).
24. Rajadhyaksha, M., Gonzalez, S., Zavislan, J.M., Anderson, R.R. & Webb, R.H. "In vivo confocal scanning laser microscopy of human skin II: advances in instrumentation and comparison with histology". *J Invest Dermatol* **113**, 293–303 (1999).
25. Sabharwal, Y.S., Rouse, A.R., Donaldson, L., Hopkins, M.F. & Gmitro, A.F. "Slit-scanning confocal microendoscope for high-resolution in vivo imaging". *Appl Opt* **38**, 7133–7144 (1999).
26. Sakashita, M., Inoue, H., Kashida, H., Tanaka, J., Cho, J.Y., Satodate, H., Hidaka, E., Yoshida, T., Fukami, N., Tamegai, Y., Shiokawa, A. & Kudo, S. "Virtual histology of colorectal lesions using laser-scanning confocal microscopy". *Endoscopy* **35**, 1033–1038 (2003).
27. Thiberville, L., Moreno-Swirc, S., Vercauteren, T., Peltier, E., Cave, C. & Bourg Heckly, G. "In vivo imaging of the bronchial wall microstructure using fibered confocal fluorescence microscopy". *Am J Respir Crit Care Med* **175**, 22–31 (2007).
28. Wang, T.D., Mandella, M.J., Contag, C.H. & Kino, G.S. "Dual-axis confocal microscope for high-resolution in vivo imaging". *Optics letters* **28**, 414–416 (2003).
29. Wiesner, C., Jager, W., Salzer, A., Biesterfeld, S., Kiesslich, R., Hampel, C., Thuroff, J.W. & Goetz, M. "Confocal laser endomicroscopy for the diagnosis of urothelial bladder neoplasia: a technology of the future?". *BJU Int* **107**, 399–403 (2011).
30. Giniunas, L., Juskaitis, R. & Shatalin, S.V. "Endoscope with optical sectioning capability". *Appl Opt* **32**, 2888–2890 (1993).
31. Kim, P., Chung, E., Yamashita, H., Hung, K.E., Mizoguchi, A., Kucherlapati, R., Fukumura, D., Jain, R.K. & Yun, S.H. "In vivo wide-area cellular imaging by side-view endomicroscopy". *Nature methods* **7**, 303–305 (2010).
32. Pillai, R.S., Lorenser, D. & Sampson, D.D. "Deep-tissue access with confocal fluorescence microendoscopy through hypodermic needles". *Opt Express* **19**, 7213–7221 (2011).
33. Koenig, F., Knittel, J. & Stepp, H. "Diagnosing cancer in vivo". *Science* **292**, 1401–1403 (2001).
34. Lane, P.M., Lam, S., McWilliams, A., Leriche, J.C., Anderson, M.W. & Macaulay, C.E. "Confocal fluorescence microendoscopy of bronchial epithelium". *J Biomed Opt* **14**, 024008 (2009).
35. Gmitro, A.F. & Aziz, D. "Confocal microscopy through a fiber-optic imaging bundle". *Optics letters* **18**, 565 (1993).
36. Farahati, B., Stachs, O., Prall, F., Stave, J., Guthoff, R., Pau, H.W. & Just, T. "Rigid confocal endoscopy for in vivo imaging of experimental oral squamous intra-epithelial lesions". *Journal of oral pathology & medicine : official publication of the International Association of Oral Pathologists and the American Academy of Oral Pathology* **39**, 318–327 (2010).
37. Kumar, K., Avritscher, R., Wang, Y., Lane, N., Madoff, D.C., Yu, T.K., Uhr, J.W. & Zhang, X. "Handheld histology-equivalent sectioning laser-scanning confocal optical microscope for interventional imaging". *Biomedical microdevices* **12**, 223–233 (2010).
38. Shin, H.J., Pierce, M.C., Lee, D., Ra, H., Solgaard, O. & Richards-Kortum, R. "Fiber-optic confocal microscope using a MEMS scanner and miniature objective lens". *Opt Express* **15**, 9113–9122 (2007).
39. Goetz, M. & Kiesslich, R. "Advances of endomicroscopy for gastrointestinal physiology and diseases". *Am J Physiol Gastrointest Liver Physiol* **298**, G797–806 (2010).

40. Goetz, M. & Kiesslich, R. "Confocal endomicroscopy: in vivo diagnosis of neoplastic lesions of the gastrointestinal tract". *Anticancer research* **28**, 353–360 (2008).
41. Paull, P.E., Hyatt, B.J., Wassef, W. & Fischer, A.H. "Confocal laser endomicroscopy: a primer for pathologists". *Archives of pathology & laboratory medicine* **135**, 1343–1348 (2011).
42. Hoffman, A., Goetz, M., Vieth, M., Galle, P.R., Neurath, M.F. & Kiesslich, R. "Confocal laser endomicroscopy: technical status and current indications". *Endoscopy* **38**, 1275–1283 (2006).
43. Goetz, M., Hoffman, A., Galle, P.R., Neurath, M.F. & Kiesslich, R. "Confocal laser endoscopy: new approach to the early diagnosis of tumors of the esophagus and stomach". *Future Oncol* **2**, 469–476 (2006).
44. Kiesslich, R., Hoffman, A., Goetz, M., Biesterfeld, S., Vieth, M., Galle, P.R. & Neurath, M.F. "In vivo diagnosis of collagenous colitis by confocal endomicroscopy". *Gut* **55**, 591–592 (2006).
45. Nakao, M., Yoshida, S., Tanaka, S., Takemura, Y., Oka, S., Yoshihara, M. & Chayama, K. "Optical biopsy of early gastroesophageal cancer by catheter-based reflectance-type laser-scanning confocal microscopy". *Journal of biomedical optics* **13**, 054043 (2008).
46. Pitris, C., Bouma, B., Shiskov, M. & Tearney, G. "A GRISM-based probe for spectrally encoded confocal microscopy". *Opt Express* **11**, 120–124 (2003).
47. Yelin, D., Boudoux, C., Bouma, B.E. & Tearney, G.J. "Large area confocal microscopy". *Optics letters* **32**, 1102–1104 (2007).
48. Becker, V., Vercauteren, T., von Weyhern, C.H., Prinz, C., Schmid, R.M. & Meining, A. "High-resolution miniprobe-based confocal microscopy in combination with video mosaicing (with video)". *Gastrointest Endosc* **66**, 1001–1007 (2007).
49. Patel, Y.G., Nehal, K.S., Aranda, I., Li, Y., Halpern, A.C. & Rajadhyaksha, M. "Confocal reflectance mosaicing of basal cell carcinomas in Mohs surgical skin excisions". *Journal of biomedical optics* **12**, 034027 (2007).
50. Kang, D., Yoo, H., Jillella, P., Bouma, B.E. & Tearney, G.J. "Comprehensive volumetric confocal microscopy with adaptive focusing". *Biomed Opt Express* **2**, 1412–1422 (2011).
51. Kang, D.K., Pal, P., Carruth, R.W., Schlachter, S., Bouma, B.E., Tearney, G.J. Esophageal endoscopic probe optica for spectrally encoded confocal microscopy using a multimode, large-core, optical fiber. in *SPIE Photonics West* (San Francisco, CA, 2012).
52. Suter, M.J., Vakoc, B.J., Yachimski, P.S., Shishkov, M., Lauwers, G.Y., Mino-Kenudson, M., Bouma, B.E., Nishioka, N.S. & Tearney, G.J. "Comprehensive microscopy of the esophagus in human patients with optical frequency domain imaging". *Gastrointest Endosc* **68**, 745–753 (2008).
53. Tearney, G.J., Waxman, S., Shishkov, M., Vakoc, B.J., Suter, M.J., Freilich, M.I., Desjardins, A.E., Oh, W.Y., Bartlett, L.A., Rosenberg, M. & Bouma, B.E. "Three-dimensional coronary artery microscopy by intracoronary optical frequency domain imaging". *JACC Cardiovasc Imaging* **1**, 752–761 (2008).
54. Yun, S., Tearney, G., de Boer, J., Iftimia, N. & Bouma, B. "High-speed optical frequency-domain imaging". *Opt Express* **11**, 2953–2963 (2003).
55. Brezinski, M.E., Tearney, G.J., Boppart, S.A., Swanson, E.A., Southern, J.F. & Fujimoto, J.G. "Optical biopsy with optical coherence tomography: feasibility for surgical diagnostics". *J Surg Res* **71**, 32–40 (1997).
56. Chinn, S.R., Swanson, E.A. & Fujimoto, J.G. "Optical coherence tomography using a frequency-tunable optical source". *Optics letters* **22**, 340–342 (1997).
57. Fujimoto, J.G., Brezinski, M.E., Tearney, G.J., Boppart, S.A., Bouma, B., Hee, M.R., Southern, J.F. & Swanson, E.A. "Optical biopsy and imaging using optical coherence tomography". *Nat Med* **1**, 970–972 (1995).
58. Tearney, G.J., Brezinski, M.E., Bouma, B.E., Boppart, S.A., Pitris, C., Southern, J.F. & Fujimoto, J.G. "In vivo endoscopic optical biopsy with optical coherence tomography". *Science* **276**, 2037–2039 (1997).
59. Tearney, G.J., Brezinski, M.E., Southern, J.F., Bouma, B.E., Boppart, S.A. & Fujimoto, J.G. "Optical biopsy in human gastrointestinal tissue using optical coherence tomography". *Am J Gastroenterol* **92**, 1800–1804 (1997).
60. Tearney, G.J., Brezinski, M.E., Southern, J.F., Bouma, B.E., Boppart, S.A. & Fujimoto, J.G. "Optical biopsy in human urologic tissue using optical coherence tomography". *J Urol* **157**, 1915–1919 (1997).
61. Leitgeb, R., Hitzenberger, C. & Fercher, A. "Performance of fourier domain vs. time domain optical coherence tomography". *Opt Express* **11**, 889–894 (2003).
62. Choma, M., Sarunic, M., Yang, C. & Izatt, J. "Sensitivity advantage of swept source and Fourier domain optical coherence tomography". *Opt Express* **11**, 2183–2189 (2003).
63. Goodman, J.W. & Rawson, E.G. "Statistics of modal noise in fibers: a case of constrained speckle". *Opt Lett* **6**, 324–326 (1981).
64. Goodman, J.W. *Speckle Phenomena in Optics: Theory and Applications*, (Roberts and Company, 2006).
65. Cogswell, C.J., Hamilton, D. K., Sheppard, C. J. R. "Colour confocal reflection microscopy using red, green and blue lasers". *Journal of Microscopy* **165**, 103–117 (1992).
66. Connor Davenport, C.M., Gmitro, A. F. Angioscopic fluorescence imaging system. in *Optical Fibers in Medicine VII*, Vol. 1649 (ed. Katzir, A.) 192–202 (SPIE, Los Angeles, CA, 1992).
67. Ellis, G.W. Scanned aperture light microscopy. in *Proceedings of the 46th Annual Meeting of EMSA* 48-49 (San Francisco Press Inc., San Francisco, 1988).
68. Yun, S.H., Richardson, D.J. & Kim, B.Y. "Interrogation of fiber grating sensor arrays with a wavelength-swept fiber laser". *Optics letters* **23**, 843–845 (1998).
69. Yelin, D., Bouma, B.E., Yun, S.H. & Tearney, G.J. "Double-clad fiber for endoscopy". *Optics letters* **29**, 2408–2410 (2004).

70. Yelin, D., Rizvi, I., White, W.M., Motz, J.T., Hasan, T., Bouma, B.E. & Tearney, G.J. "Three-dimensional miniature endoscopy". *Nature* **443**, 765 (2006).
71. Yelin, D., White, W.M., Motz, J.T., Yun, S.H., Bouma, B.E. & Tearney, G.J. "Spectral-domain spectrally-encoded endoscopy". *Opt Express* **15**, 2432–2444 (2007).
72. Pal, P., Kang, DongKyun, Bouma, Brett E., Tearney, Guillermo J. "Reduced speckle, large-area, comprehensive imaging by spectrally encoded confocal microscopy." *SPIE Photonics West* (SPIE, San Francisco, CA, 2011).
73. Wilson, T. & Carlini, A.R. "Size of the detector in confocal imaging systems". *Opt Lett* **12**, 227–229 (1987).
74. Lemire-Renaud, S., Rivard, M., Strupler, M., Morneau, D., Verpillat, F., Daxhelet, X., Godbout, N. & Boudoux, C. "Double-clad fiber coupler for endoscopy". *Opt Express* **18**, 9755–9764 (2010).
75. Lemire-Renaud, S., Strupler, M., Benboujja, F., Godbout, N. & Boudoux, C. "Double-clad fiber with a tapered end for confocal endomicroscopy". *Biomed Opt Express* **2**, 2961–2972 (2011).
76. Kang, D.K., Pal, P., Carruth, R. W., Schlachter, S., Bouma, B.E., Tearney, G.J. Esophageal endoscopic probe optics for spectrally encoded confocal microscopy using a multimode, large-core, optical fiber. in *SPIE Photonics West* (SPIE, San Francisco, CA, 2012).
77. Alfano, R.R., Shapiro, S. L. "Emission in the region 4000 to 7000 A via four-photon coupling in glass". *Physical Review Letters* **24**, 584–587 (1970a).
78. Lin, C. & Stolen, R.H. "New Nanosecond Continuum for Excited-State Spectroscopy". *Applied Physics Letters* **28**, 216–218 (1976).
79. Russell, P. "Photonic crystal fibers". *Science* **299**, 358–362 (2003).
80. Jones, R.J., Moll, K.D., Thorpe, M.J. & Ye, J. "Phase-coherent frequency combs in the vacuum ultraviolet via high-harmonic generation inside a femtosecond enhancement cavity". *Physical Review Letters* **94**, - (2005).
81. Aguirre, A.D., Nishizawa, N., Fujimoto, J.G., Seitz, W., Lederer, M. & Kopf, D. "Continuum generation in a novel photonic crystal fiber for ultrahigh resolution optical coherence tomography at 800 nm and 1300 nm". *Optics Express* **14**, 1145–1160 (2006).
82. Aguergaray, C., Andersen, T.V., Schimpf, D.N., Schmidt, O., Rothhardt, J., Schreiber, T., Limpert, J., Cormier, E. & Tunnermann, A. "Parametric amplification and compression to ultrashort pulse duration of resonant linear waves". *Optics Express* **15**, 5699–5710 (2007).
83. Boudoux, C., Yun, S., Oh, W., White, W., Iftimia, N., Shishkov, M., Bouma, B. & Tearney, G. "Rapid wavelength-swept spectrally encoded confocal microscopy". *Opt Express* **13**, 8214–8221 (2005).
84. Oh, W.Y., Yun, S.H., Tearney, G.J. & Bouma, B.E. "115 kHz tuning repetition rate ultrahigh-speed wavelength-swept semiconductor laser". *Optics letters* **30**, 3159–3161 (2005).
85. Yun, S.H., Boudoux, C., Pierce, M.C., de Boer, J.F., Tearney, G.J. & Bouma, B.E. "Extended-Cavity Semiconductor Wavelength-Swept Laser for Biomedical Imaging". *IEEE Photonics Technol Lett* **16**, 293–295 (2004).
86. Yun, S.H., Boudoux, C., Tearney, G.J. & Bouma, B.E. "High-speed wavelength-swept semiconductor laser with a polygon-scanner-based wavelength filter". *Opt Lett* **28**, 1981–1983 (2003).
87. Campo-Ruiz, V., Patel, D., Anderson, R.R., Delgado-Baeza, E. & Gonzalez, S. "Virtual biopsy of the joint tissues using near-infrared, reflectance confocal microscopy. A pilot study". *Microsc Res Tech* **69**, 794–798 (2006).
88. Gonzalez, S., Rajadhyaksha, M., Rubinstein, G. & Anderson, R.R. "Characterization of psoriasis in vivo by reflectance confocal microscopy". *J Med* **30**, 337–356 (1999).
89. Luck, B.L., Carlson, K.D., Bovik, A.C. & Richards-Kortum, R.R. "An image model and segmentation algorithm for reflectance confocal images of in vivo cervical tissue". *IEEE Trans Image Process* **14**, 1265–1276 (2005).
90. Tilli, M.T., Cabrera, M.C., Parrish, A.R., Torre, K.M., Sidawy, M.K., Gallagher, A.L., Makariou, E., Polin, S.A., Liu, M.C. & Furth, P.A. "Real-time imaging and characterization of human breast tissue by reflectance confocal microscopy". *Journal of biomedical optics* **12**, 051901 (2007).
91. Yoo, H., Kang, D., Katz, A.J., Lauwers, G.Y., Nishioka, N.S., Yagi, Y., Tanpowpong, P., Namati, J., Bouma, B.E. & Tearney, G.J. "Reflectance confocal microscopy for the diagnosis of eosinophilic esophagitis: a pilot study conducted on biopsy specimens". *Gastrointest Endosc* **74**, 992–1000 (2011).
92. Sung, K.B., Richards-Kortum, R., Follen, M., Malpica, A., Liang, C. & Descour, M. "Fiber optic confocal reflectance microscopy: a new real-time technique to view nuclear morphology in cervical squamous epithelium in vivo". *Opt Express* **11**, 3171–3181 (2003).
93. Kang, D., Suter, M.J., Boudoux, C., Yoo, H., Yachimski, P.S., Puricelli, W.P., Nishioka, N.S., Mino-Kenudson, M., Lauwers, G.Y., Bouma, B.E. & Tearney, G.J. "Comprehensive imaging of gastroesophageal biopsy samples by spectrally encoded confocal microscopy". *Gastrointest Endosc* **71**, 35–43 (2010).
94. Kang, D.K., Suter, M.J., Boudoux, C., Yachimski, P.S., Puricelli, W.P., Nishioka, N.S., Mino-Kenudson, M., Lauwers, G.Y., Bouma, B.E. & Tearney, G.J. "Co-registered spectrally encoded confocal microscopy and optical frequency domain imaging system". *J Microsc* **239**, 87–91 (2010).
95. Cense, B., Chen, T.C., Nassif, N., Pierce, M.C., Yun, S.H., Park, B.H., Bouma, B.E., Tearney, G.J. & de Boer, J.F. "Ultra-high speed and ultra-high resolution spectral-domain optical coherence tomography and optical Doppler tomography in ophthalmology". *Bull Soc Belge Ophtalmol*, 123–132 (2006).
96. Cense, B., Chen, T.C. & de Boer, J.F. "In vivo thickness and birefringence determination of the human retinal nerve fiber layer using polarization-sensitive optical coherence tomography". *Bull Soc Belge Ophtalmol*, 109–121 (2006).
97. Lim, H., Mujat, M., Kerbage, C., Lee, E.C., Chen, Y., Chen, T.C. & de Boer, J.F. "High-speed imaging of human retina

in vivo with swept-source optical coherence tomography". *Opt Express* **14**, 12902–12908 (2006).

98. You, J.W., Chen, T.C., Mujat, M., Park, B.H. & de Boer, J.F. "Pulsed illumination spectral-domain optical coherence tomography for human retinal imaging". *Opt Express* **14**, 6739–6748 (2006).
99. Chen, T.C., Cense, B., Miller, J.W., Rubin, P.A., Deschler, D.G., Gragoudas, E.S. & de Boer, J.F. "Histologic correlation of in vivo optical coherence tomography images of the human retina". *American journal of ophthalmology* **141**, 1165–1168 (2006).
100. Tao, Y.K., Farsiu, S. & Izatt, J.A. "Interlaced spectrally encoded confocal scanning laser ophthalmoscopy and spectral domain optical coherence tomography". *Biomed Opt Express* **1**, 431–440 (2010).
101. Tao, Y.K. & Izatt, J.A. "Spectrally encoded confocal scanning laser ophthalmoscopy". *Opt Lett* **35**, 574–576 (2010).
102. Kiesslich, R., Kanzler, S., Vieth, M., Moehler, M., Neidig, J., Thanka Nadar, B.J., Schilling, D., Burg, J., Nafe, B., Neurath, M.F. & Galle, P.R. "Minimal change esophagitis: prospective comparison of endoscopic and histological markers between patients with non-erosive reflux disease and normal controls using magnifying endoscopy". *Dig Dis* **22**, 221–227 (2004).
103. Noel, R.J., Putnam, P.E., Collins, M.H., Assa'ad, A.H., Guajardo, J.R., Jameson, S.C. & Rothenberg, M.E. "Clinical and immunopathologic effects of swallowed fluticasone for eosinophilic esophagitis". *Clin Gastroenterol Hepatol* **2**, 568–575 (2004).
104. Noel, R.J., Putnam, P.E. & Rothenberg, M.E. "Eosinophilic esophagitis". *N Engl J Med* **351**, 940-941 (2004).
105. Gupta, S.K. "Noninvasive markers of eosinophilic esophagitis". *Gastrointest Endosc Clin N Am* **18**, 157–167; xi (2008).
106. Kapel, R.C., Miller, J.K., Torres, C., Aksoy, S., Lash, R. & Katzka, D.A. "Eosinophilic esophagitis: a prevalent disease in the United States that affects all age groups". *Gastroenterology* **134**, 1316–1321 (2008).
107. Liacouras, C.A. "Eosinophilic esophagitis". *Gastroenterol Clin North Am* **37**, 989–998, xi (2008).
108. Liacouras, C.A. "Pharmacologic treatment of eosinophilic esophagitis". *Gastrointest Endosc Clin N Am* **18**, 169–178; xi (2008).
109. Atkins, D., Kramer, R., Capocelli, K., Lovell, M. & Furuta, G.T. "Eosinophilic esophagitis: the newest esophageal inflammatory disease". *Nat Rev Gastroenterol Hepatol* **6**, 267–278 (2009).
110. Franciosi, J.P., Tam, V., Liacouras, C.A. & Spergel, J.M. "A case-control study of sociodemographic and geographic characteristics of 335 children with eosinophilic esophagitis". *Clin Gastroenterol Hepatol* **7**, 415–419 (2009).
111. Moawad, F.J., Veerappan, G.R. & Wong, R.K. "Eosinophilic esophagitis". *Dig Dis Sci* **54**, 1818–1828 (2009).
112. Veerappan, G.R., Perry, J.L., Duncan, T.J., Baker, T.P., Maydonovitch, C., Lake, J.M., Wong, R.K. & Osgard, E.M. "Prevalence of eosinophilic esophagitis in an adult population undergoing upper endoscopy: a prospective study". *Clin Gastroenterol Hepatol* **7**, 420–426, 426 e421–422 (2009).
113. Markowitz, J.E., Spergel, J.M., Ruchelli, E. & Liacouras, C.A. "Elemental diet is an effective treatment for eosinophilic esophagitis in children and adolescents". *Am J Gastroenterol* **98**, 777–782 (2003).
114. Unglert, C.I., Namati, E., Warger, W.C., 2nd, Liu, L., Yoo, H., Kang, D., Bouma, B.E. & Tearney, G.J. "Evaluation of optical reflectance techniques for imaging of alveolar structure". *Journal of biomedical optics* **17**, 071303 (2012).
115. Ritman, E.L. "Micro-computed tomography of the lungs and pulmonary-vascular system". *Proc Am Thorac Soc* **2**, 477–480, 501 (2005).
116. Tsia, K.K., Goda, K., Capewell, D. & Jalali, B. "Simultaneous mechanical-scan-free confocal microscopy and laser microsurgery". *Opt Lett* **34**, 2099–2101 (2009).
117. Golan, L., Yeheskely-Hayon, D., Minai, L., Dann, E.J. & Yelin, D. "Noninvasive imaging of flowing blood cells using label-free spectrally encoded flow cytometry". *Biomed Opt Express* **3**, 1455–1464 (2012).
118. Gora, M.J., Sauk, J.S., Carruth, R.W., Gallagher, K.A., Suter, M.J., Nishioka, N.S., Kava, L.E., Rosenberg, M., Bouma, B.E. & Tearney, G.J. "Tethered capsule endomicroscopy enables less invasive imaging of gastrointestinal tract microstructure". *Nat Med* **19**, 238–240 (2013).

Parama Pal is currently a Member, Technical Staff at the Robert Bosch Centre for Cyber Physical Systems at the Indian Institute of Science. She obtained her M.Sc. in Physics from IIT Delhi in 2004 and Ph.D. in Optics from The Institute of Optics, University of Rochester in 2009. Her thesis was centered on the design and fabrication of post-processed optical fibers and their subsequent applications for laser systems and microphotonic components. From 2009–2012, she was a Research Fellow at the Wellman Center for Photomedicine, Massachusetts General Hospital and the Harvard Medical School.